[101] Oriented $Pr_{0.7}Ca_{0.3-x}Sr_xMnO_{3-\delta}$ Thin Films Prepared by rf Magnetron Reactive Sputtering

B. Mercey,* P. Lecoeur, M. Hervieu, J. Wolfman, C. Simon, H. Murray, and B. Raveau

Laboratoire CRISMAT ISMRA Université de Caen, Boulevard du Maréchal Juin, F14050 Caen Cedex, France

Received November 5, 1996. Revised Manuscript Received February 24, 1997[⊗]

Thin films of manganite materials ($Pr_{0.7}Ca_{0.3-x}Sr_xMnO_{3-\delta}$) have been grown, from a sintered target with the same cationic composition, by rf reactive magnetron sputtering. The film and target compositions have been verified as identical, within experimental errors, by energy-dispersive scattering (EDS) analysis. It is shown for the first time, from X-ray and electron diffraction studies, that the films, grown on $LaAlO_3$ or $SrTiO_3$ substrates, are [101] oriented. Nanostructural studies show that the defects are the same as those observed in bulk materials but that the magnetic behavior is different (Curie temperature is decreased from 130 to 50K). From a structural point of view this difference in magnetic behavior is difficult to understand, but the role of the oxygen content, the small grain size observed in such films, and the strains induced by the substrate film interactions is discussed.

Introduction

The great interest in giant magnetoresistance (GMR) manganites for the realization of device applications has led to many investigations of these perovskites dealing with polycrystalline materials as well as with single crystals and thin films.

Within the scope of magnetic applications, the deposition of such thin films with optimal GMR properties is of high importance. To date, the main results concern thin films prepared by laser ablation.[1−9] The control of the growth of these films was revealed to be difficult, due to oxygen nonstoichiometry and crystallization problems. For this reason, the as-grown film is sometimes annealed in an oxygen flow at a temperature higher than that used in the growth process, to improve the GMR properties. In fact, recent structural studies performed on polycrystalline ceramics by neutron diffraction[10,11] and high-resolution electron microscopy[12] showed that the structure, and especially the nanostructure, does play a key role in the GMR properties of these materials.

In a recent study of the manganese perovskites $Pr_{0.7}Ca_{0.3-x}Sr_xMnO_3$, exceptional resistance ratios ranging from 10^5 to 10^{11} at temperatures of 88 and 30 K, respectively, were observed for polycrystalline ceramics.[13,14] The HREM study of this material evidenced complex structural phenomena, involving a breakdown of the usual *Pnma* symmetry and the formation of isolated "pointlike defects" suggesting a local charge ordering.[15] The realization of such films, with large areas should be of interest in view of applications. We report herein on the growth of $Pr_{0.7}Ca_{0.3-x}Sr_xMnO_{3-\delta}$ thin films ($x = 0.05$ and 0.08), deposited by rf magnetron reactive sputtering, which is not an usual deposition technique for GMR manganites.[16] The [101] orientation of such films is evidenced for the first time, and their detailed HREM study presented.

Experimental Section

Targets Preparation. Considering the system $Pr_{0.7}Ca_{0.3-x}Sr_xMnO_3$, targets were prepared by solid-state reaction, starting from stoichiometric amounts of Pr_6O_{11}, $SrCO_3$, $CaCO_3$, and Mn_2O_3, with $x = 0.05$ and $x = 0.08$. The starting reagents were mixed with an attrition milling using ZrO_2 beads in an ethanol slurry. The resulting mixtures were then filtered to eliminate the ZrO_2 beads and dried. After grinding in an agate mortar, the powders were heated to 900 °C in an alumina boat, held at this temperature during 15 h and then cooled to room temperature. The powders were ground again and subjected to a second similar heat treatment. At this point, the weight losses correspond to a complete decarbonation. The resulting mixtures were carefully pulverized and then pressed into a

[⊗] Abstract published in *Advance ACS Abstracts,* April 1, 1997.

(1) von Helmolt, R.; Wecker, J.; Holzapfel, R.; Schultz, L.; Samwer, K. *Phys. Rev. Lett.* **1993**, *71*, 2331.
(2) McCormack, M.; Jin, S.; Tiefel, T. H.; Fleming, R. M.; Phillips, J. M.; Ramesh, R. *Appl. Phys. Lett.* **1994**, *64*, 3045.
(3) Ju, H. L.; Kwon, C.; Li, Q.; Greene, R. L.; Venkatesan, T. *Appl. Phys. Lett.* **1994**, *65*, 2108.
(4) von Helmolt, R.; Wecker, J.; Samwer, K.; Haupt, L.; Barner, K. *J. Appl. Phys.* **1994**, *76*, 6925.
(5) Xiong, G. C.; Li, Q.; Ju, H. L.; Mao, S. N.; Senapati, L.; Xi, X. X.; Greene, R. L.; Venkatesan, T. *Appl. Phys. Lett.* **1995**, *66*, 1427.
(6) Sun, J. Z.; Krusin-Elbaum, L.; Parkin, S. S. P.; Xiao, G. *Appl. Phys. Lett.* **1995**, *67*, 2726.
(7) Xiong, G. C.; Bhagat, S. M.; Li, Q.; Dominguez, M.; Ju, H. L.; Greene, R. L.; Venkatesan, T.; Byers, J. M.; Rubinstein, M. *Solid State Commun.* **1996**, *97*, 599.
(8) Canedy, C. L.; Ibsen, K. B.; Xiao, G.; Sun, J. Z.; Gupta, A.; Gallagher, J. *J. Appl. Phys.* **1996**, *79*, 4546.
(9) McGuire, T. R.; Gupta, A.; Duncombe, P. R.; Rupp, M.; Sun, J. Z.; Laibowitz, R. B.; Gallagher, J.; Xiao, G. *J. Appl. Phys.* **1996**, *79*, 4549.
(10) Caignaert, V.; Suard, E.; Maignan, A.; Simon, C.; Raveau, B. *J. Magn. Magn. Mater.* **1996**, *153*, L260.
(11) Yoshizawa, H.; Kawano, H.; Tomioka, Y.; Tokura, Y. *Phys. Rev. B* **1995**, *52*, 13145.
(12) Laffez, P.; Van Tendeloo, G.; Millange, F.; Caignaert, V.; Hervieu, M.; Raveau, B. *Mater. Res. Bull.* **1996**, *31*, 905.
(13) Maignan, A.; Simon, C.; Caignaert, V.; Raveau, B. *Solid State Commun.* **1995**, *96*, 623.
(14) Raveau, B.; Maignan, A.; Caignaert, V. *J. Solid State Chem.* **1995**, *117*, 424.
(15) Hervieu, M.; Van Tendeloo, G.; Caignaert, V.; Maignan, A.; Raveau, B. *Phys. Rev. B* **1996**, *53*, 14274.
(16) Nunez-Regueiro, J. E.; Gupta, D.; Kadin, A. M. *J. Appl. Phys.* **1996**, *79*, 5179.

S0897-4756(96)00572-8 CCC: $14.00

pellet (2.5 cm diameter). The pellets were slowly heated to 1500 °C, isothermed for 20 h, and then slowly cooled. X-ray diffraction of the sintered targets allowed to check the targets are single-phased with perovskite-like structures.

Thin-Film Deposition. The sintered target was polished and then glued with silver paste to a 1 in. magnetron sputtering source (Torus 1C, K. J. Lesker). The sputtering source was mounted in an Alcatel SCM 450 deposition system. This deposition system was evacuated with a rotary and a turbomolecular pumping unit (pressure limit 5×10^{-7} Torr). The substrate ($LaAlO_3$ [001] or $SrTiO_3$ [001]) was glued with silver paste to a stainless steel heater block facing the target. The temperature of the substrate was varied from 650 to 750 °C. During deposition, pressure inside the chamber, controlled by a butterfly valve, was 0.15 Torr. The plasma gas was composed of argon and oxygen, oxygen concentration varying between 0.5 and 3%. The gas flow and the ratio between argon and oxygen were controlled by mass flow controllers. During deposition the rf power was 70 or 50 W and deposition duration was 30 min. After deposition the chamber was filled with oxygen (1 atm), and then the heater block was slowly cooled to room temperature.

Characterization. The films were characterized by X-ray diffraction (XRD) with a Seifert diffractometer, θ-2θ mode, using Cu $K\alpha_1$ radiation. Transmission electron microscopy (TEM) was performed with a JEOL 200CX electron microscope equipped with a eucentric goniometer (±60°) and high-resolution electron microscopy (HREM) with a Topcon 002B microscope having a point resolution of 1.8 Å. The thin film was observed in a direction perpendicular to the substrate. Image calculations were carried out with the Mac Tempas program. Fourier transformations were performed, from digitized images, with an NIH image program.The composition of the films was measured by energy-dispersive scattering (EDS) with Kevex analyzer mounted on each microscope. Magnetic behavior was measured with a Quantum Design Model MPMS1 SQUID magnetometer.

Results

Optimization of the Thin-Films Deposition. From previous work performed in our laboratory by rf reactive sputtering[17] we knew that the crystallization of a film with the same cationic composition as the ceramic sintered target is not straightforward. To ensure the conservation of the stoichiometry between target (i.e., $Pr_{0.7}Ca_{0.3-x}Sr_xMnO_3$) and deposited film, a possible route is to prepare the films using a plasma gas with the lowest oxygen concentration needed for deposition of oxides. First experiments were carried out with an oxygen concentration varying between 0.5 and 3%; the other plasma gas was argon. From XRD experiments, it appeared that the films that gave the best diffraction patterns were obtained for an oxygen concentration of 0.5%, a pressure during deposition of 0.15 mbar, and a substrate heater temperature of 715 °C. Despite the "in situ" annealing performed at the same temperature as the temperature deposition under 1 atm oxygen and the slow cool of the film, it appeared from XPS measurements that the ratio between Mn(III) and Mn(IV) did not correspond to the theoretical one. To promote a larger oxidation of the manganese, without using an annealing at temperature higher than the deposition temperature, the rf power was reduced from 70 to 50 W to decrease the deposition rate and ensure a more effective reaction between manganese and oxygen. The ratio between Mn(III) and Mn(IV), calculated from XPS measurements, was then closer to the theoretical one. Cationic composition of the films checked from EDS measurements was found to be the same as the target composition within the experimental errors. In Table 1 are summarized the deposition conditions leading to the growth of the best films.

Table 1. Optimized Growth Conditions of $Pr_{0.7}Ca_{0.3-x}Sr_xMnO_3$ Films

substrate	$LaAlO_3$ [001] or $SrTiO_3$ [001]
deposition temp	715 °C
gas composition	Ar 99.5%, O_2 0.5%
pressure during deposition	0.15 mbar
rf power	50 W
deposition duration	30 min
annealing under 1 atm of O_2	30 min
cool-down rate	6 °C min^{-1}

Optimized Films. *X-ray Diffraction.* The XRD patterns of the films grown under optimized conditions, on $LaAlO_3$ or $SrTiO_3$, exhibit two sharp peaks at 3.837 and 1.923 Å (Figure 1). For the same growth conditions, no variation of these peak positions are observed when using $LaAlO_3$ or $SrTiO_3$.

The orthorhombic cell parameters of the $x = 0.05$ bulk material[15] were refined to $a = 5.459$ Å ($\approx\sqrt{2}a_p$), $b = 7.683$ Å ($\approx 2a_p$), $c = 5.437$ Å ($\approx\sqrt{2}a_p$), and the conditions limiting the reflection are $0kl$, $k + l = 2n$ and $hk0$, $h = 2n$ compatible with the $Pnma$ and $Pn2a$ space groups. The a_p parameter of the perovskite subcell determined from the XRD pattern of the thin film, $a_p \approx 3.846$ Å, is in agreement with the above values, but the 3.837 and 1.923 Å interplanar distances are consistent only with a perovskite-related structure and do not display information on the cell parameters and symmetry.

Assuming the structure of the thin film is that of the bulk material, two orientations of the film with respect to the substrate plane would involve such a XRD pattern: (i) The film is [010] oriented 3.837 and 1.922 Å corresponds to the 020 and 040 reflections ($0k0$, $k = 2n$). (ii) The film is [101] oriented 3.837 and 1.919 Å are the 101 and 202 reflections.

For $x = 0.05$, the interreticular distances calculated for the bulk material are $d_{004} = 1.9208$ Å and $d_{202} = 1.9261$ Å. However, lattice parameter differences have been often observed for the same phase prepared as bulk material or in the form of thin film,[18] due to structural problems such as strains (depending on the substrate) or oxygen content variations. As a consequence, the orientation of the film with respect to the substrate could not be assumed on the simple basis of such a small distance variation. The relative orientation of the film with respect to the substrate was studied using ED and TEM.

ED Study. Viewed along a direction perpendicular to the substrate plane, the electron diffraction (ED) patterns exhibit sharp reflections and allow evidence of two structural characteristics: (i) The intense reflections correspond to a perovskite-like system, but superstructure reflections are observed that involve the periodicity $2a_p \times a_p$. (ii) Two variants of the supercell are systematically superimposed, which indicates the existence of 90° oriented domains.

Similar patterns are observed for the two optimized films, $x = 0.05$ and $x = 0.08$, whatever the type of substrate may be, $LaAlO_3$ [001] or $SrTiO_3$ [001]. An

(17) Lecoeur, P.; Mercey, B.; Murray, H. *J. Vac. Sci. Technol. A* **1995**, *13*, 2221.

(18) Geerk, J.; Linker, G.; Meyer, O. *Mater, Sci. Rep.* **1989**, *4*, 193.

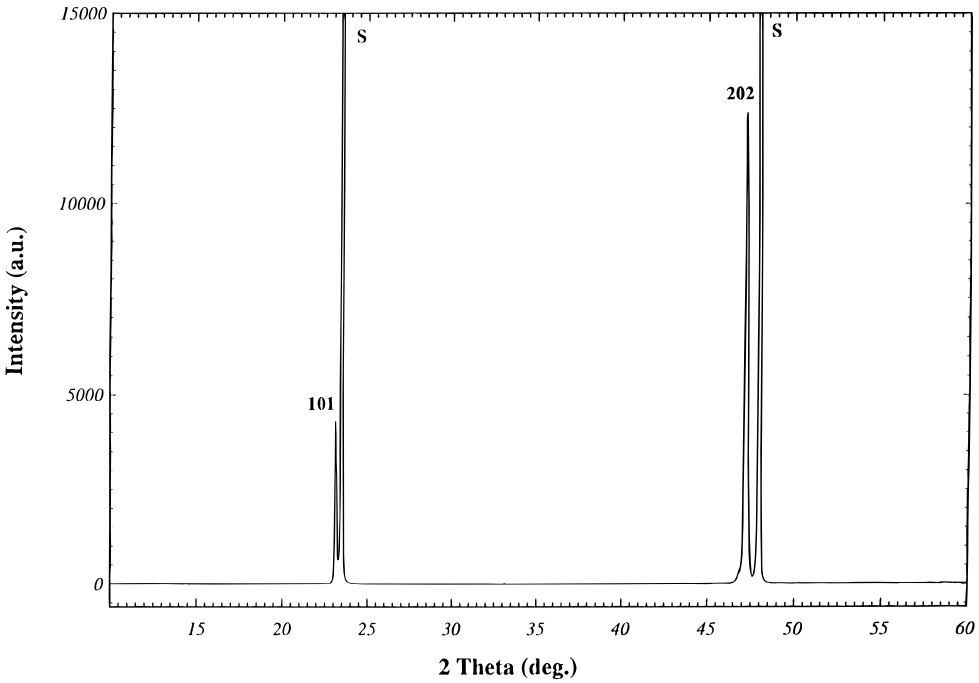

Figure 1. XRD pattern of the optimized thin film deposited on $SrTiO_3$ (peaks labeled S are the substrate peaks).

example is displayed in Figure 2a, where the two variants are subscripted 1 and 2, and drawn in Figure 2c.

Referring to the orthorhombic cell, the ED patterns show that the films are mainly [101] oriented. Since two substrates with a perovskite cell are used, this orientation could be expected because the periodicity along [010] and $[\bar{1}01]$, $2a_p$ and a_p, respectively, fit well with the substrate parameters. Taking into account the double diffraction phenomenon, this pattern is consistent with the orthorhombic cell and the reflection condition $0k0$, $k = 2n$, observed in the bulk material.

Note that extra reflections are sometimes observed in such ED patterns, recorded along a direction perpendicular to the substrate plane; they are indicated by small white arrows in Figure 2b. Such patterns are commonly observed in the bulk material; this feature is generated by the existence of domains that are [010] oriented (drawn in Figure 2c). The intensity of these extra reflections are weak, since the [010] domains always extend over very small areas (see further). The parameter relationships $a/\sqrt{2} \approx b/2 \approx c/\sqrt{2} \approx a_p$ indeed favor the existence of such perfectly oriented domains.

The reconstruction of the reciprocal space, tilting around [010]* and $[\bar{1}01]$*, allow us to confirm the cell parameters $\mathbf{a} \approx \sqrt{2}a_p$, $\mathbf{b} \approx 2a_p$, and $\mathbf{c} \approx \sqrt{2}a_p$. The conditions limiting the reflection can hardly be determined due to the systematic existence of oriented domains; however, when this determination can be carried out on larger domains, it shows that the conditions of reflection are in agreement with those observed in the bulk material, i.e., $0kl$, $k+l = 2n$, and $hk0$, $h = 2n$ (the odd $h00$, $0k0$, and $00l$ appear from double-diffraction phenomena).

The EDS analyses performed on numerous areas of the films confirm that the actual compositions are the nominal ones, i.e., correspond to the target compositions.

Film Morphology. The [101] HREM images confirm the good cristallinity of the film, in agreement with the sharpness of the reflections. The films consist of small grains which mainly exhibit a nearly square shape and are a few hundred angstroms wide. An example is shown in Figure 3, which corresponds to the $x = 0.05$ film. In this image, the $\mathbf{b}$ axis is indicated by white arrows for some of the grains (this direction is clearly observed in the HREM images; see for example Figure 4a). It appears that the grains are 90° oriented, in agreement with the ED patterns (Figure 2a) but, also, that the domain size often corresponds to the grain size, i.e., that the domains evidenced by the ED study are in fact the grains constituting the film.

In this image of the $x = 0.05$ film and in the corresponding enlarged part (Figure 4a), it can be observed that the grain boundaries (indicated by black arrows in Figure 4a) are mainly parallel to the $[010]_p$ and $[101]_p$ directions of the perovskite subcell. In the thick part of the film (right part of the image), the boundaries appear as rather perfect, but in the thinnest part of the film, it can be seen that the material is sometimes disturbed over a few angstroms. This morphology can be compared to that recorded for the film $x = 0.08$ (the two films were prepared following exactly the same growth process), which is displayed in Figure 4b. The film consists also of small 90° oriented domains, and it differs from the previous one only by the shape of the domains, which do not exhibit anymore a clear geometrical shape, and the grain (or domain) boundaries which are now "filled" up by well-crystallized material. Only small spherical but rare domains of disturbed material remain.

Nanostructural Study. A first important point is observed from these images. The through-focus series show indeed that the contrast is very similar to that observed in the bulk material and, therefore, confirms the structure-type of the manganite deposited in the form of thin film. The images were calculated, varying the focus and crystal thickness values, and previously reported and discussed in ref 15. An example of typical image is given in Figure 5, where the heavy cation positions are imaged as bright dots and the manganese as smaller gray dots (the focus value is assumed to be close to −600 Å[15]). The [010] oriented domains, which

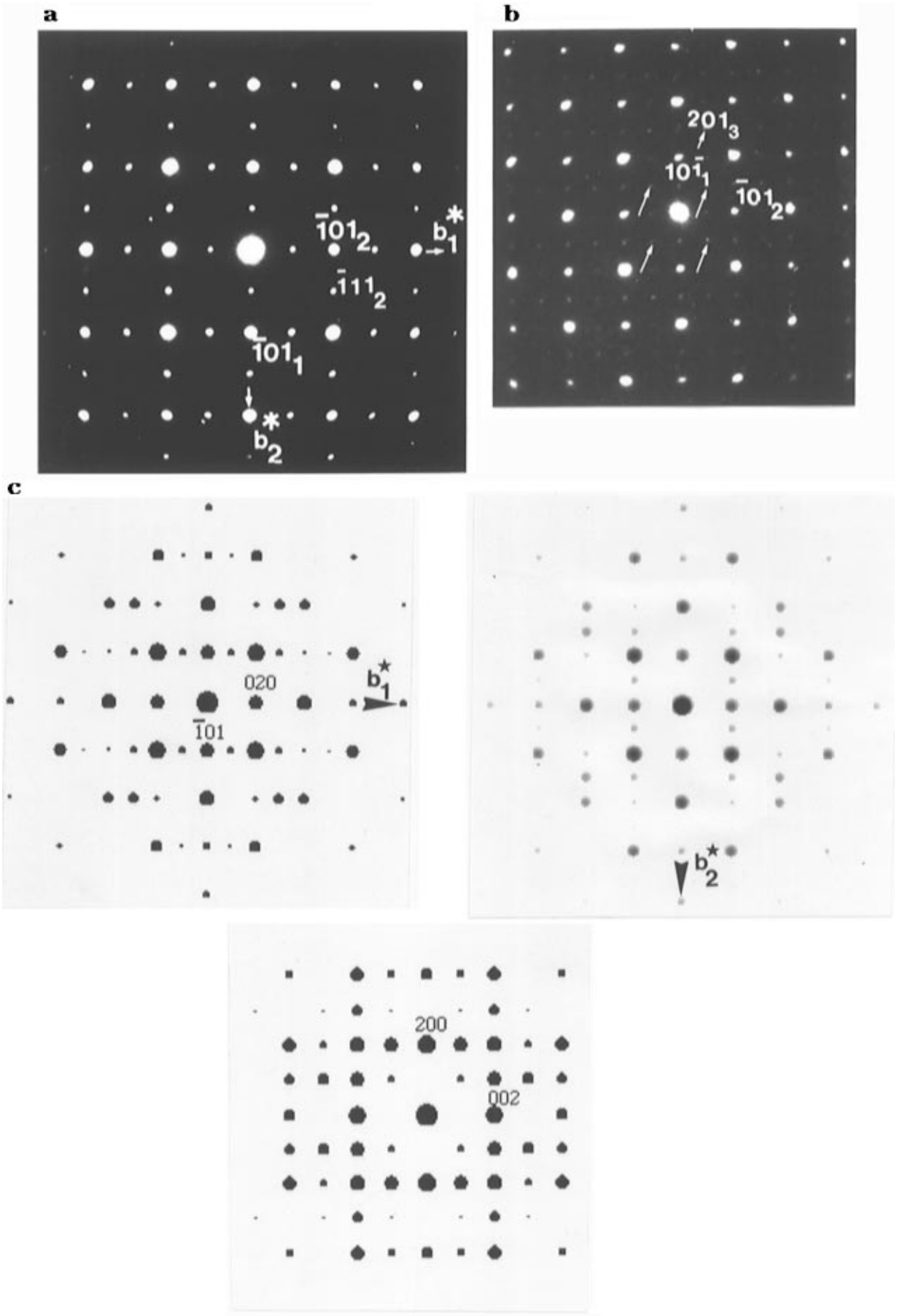

Figure 2. ED patterns recorded along a direction perpendicular to the substrate plane ($h00$, $h = 2n + 1$; $0k0$, $k = 2n + 1$, and $00l$, $l = 2n + 1$ reflections appear from double-diffraction phenomena): (a) Typical pattern showing that the film is mainly [101] oriented. The two 90° oriented variants are subscripted 1 and 2. (b) In a few patterns, extra reflections are observed (indicated by small white arrows). They arise from the existence of small [010] domains (subscripted 3). (c) Idealized drawings of the three different orientations, superposed in Figure 2b: the 90° oriented [101] patterns and [010].

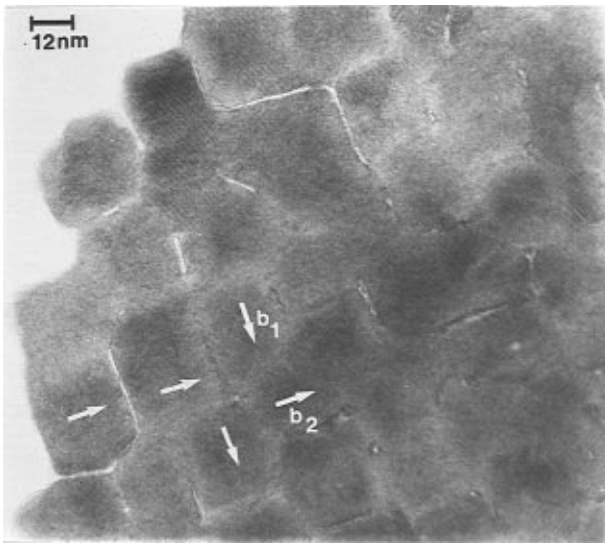

Figure 3. [101] overall image: the $Pr_{0.7}Ca_{0.25}Sr_{0.05}MnO_3$ thin film is built up from 90° oriented grains. The $\mathbf{b}$ axes are indicated for a few of them. The 90° oriented domains are subscripted 1 and 2.

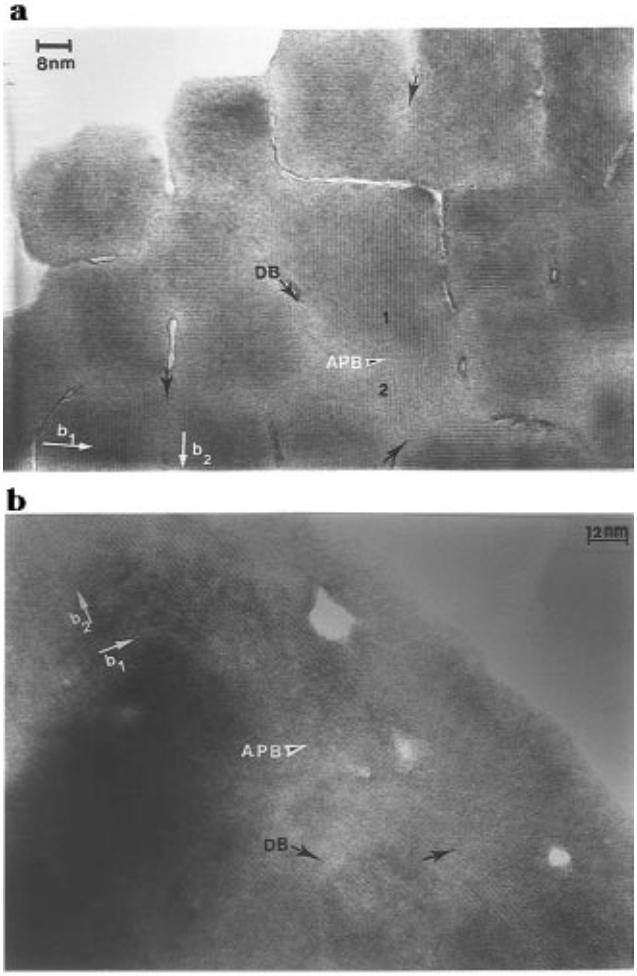

Figure 4. Enlarged [101] images of (a) $Pr_{0.7}Ca_{0.25}Sr_{0.05}MnO_3$ and of (b)$Pr_{0.7}Ca_{0.22}Sr_{0.08}MnO_3$. The domain boundaries (DB) are indicated by black arrows and the antiphase boundaries (APB) by white triangles.

give rise to extra reflections in the ED pattern recorded along the direction perpendicular to the substrate, are very small, with a maximum of a few tens of angstroms, (contrary to the bulk material) and often located close to the grain boundaries. Two examples are indicated by curved arrows in Figure 5.

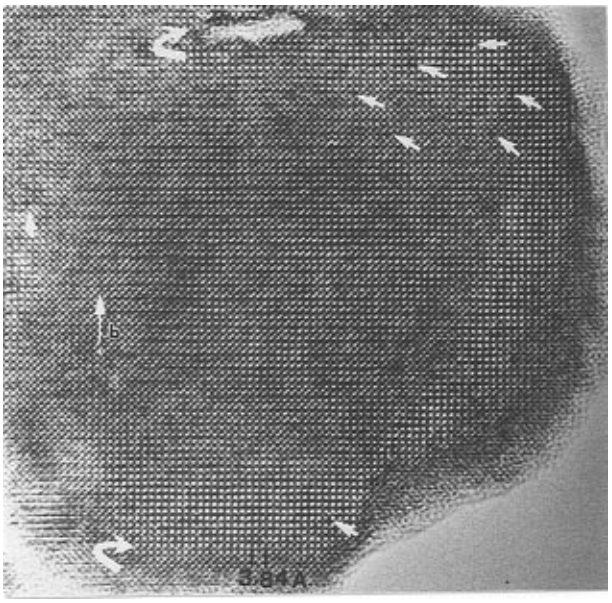

Figure 5. Enlarged [101] image where two small areas of [010] oriented manganite are observed (curved arrows). Point-like defects are indicated by small white arrows.

The second important point is that the nanostructural state of the film is also similar to that observed for the bulk material. Isolated pointlike defects that appear as brighter or darker dots depending of the focus and the thickness values are systematically observed in the matrix. As an example, they are observed as small darker dots in the crystal edge presented in Figure 5; a few of them are indicated by small white arrows. These defects were first reported in the bulk material and correlated to the existence of $A^{II}Mn^{IV}O_3$ clusters.[15] Two other types of nanostructural phenomena that were reported in the bulk material are also observed here. They are both directly related the octahedral framework distortion. They are displayed in Figure 6 where the two manganese layers appear as alternating rows of small dark and gray dots, with a periodicity of $2a_p$; they are separated by rows of bright dots correlated to the $[Ln_{1-x}A_xO]$ layers. The first type of defect corresponds to the formation of a twin boundary. At the level of the boundary (indicated by TB in Figure 6a), two rows of gray dots become adjacent: the $[Ln_{1-x}A_xO]$ layer plays therefore the role of mirror so that two equivalent manganese rows become adjacent. The [101] projection of the atom positions through the twin boundary is given in Figure 6b. Through the second type of boundary, the matrix is shifted by $b/2$, i.e., $\mathbf{t} = a_p \approx 3.85$ Å; they are interpreted as antiphase boundaries. Examples of such antiphase boundaries are indicated by the label APB in Figure 6a and drawn in Figure 6c. These phenomena were explained on the basis of the framework distortion.[15]

The existence of these defects is of importance since it emphasizes the similarity, up to the nanostructural details, of the manganite films and the ceramics.

Role of the Deposition Parameters. The XRD characterization of the films shows that most of the different parameters of the deposition process plays a role for the film quality. To understand these points, the morphology and the nanostructural state of different $Pr_{0.7}Ca_{0.22}Sr_{0.08}MnO_3$ films were studied, varying only one parameter per experiment: (i) Film F_1: the oxygen concentration $p_{O_2} = 1\%$, retaining the other growth

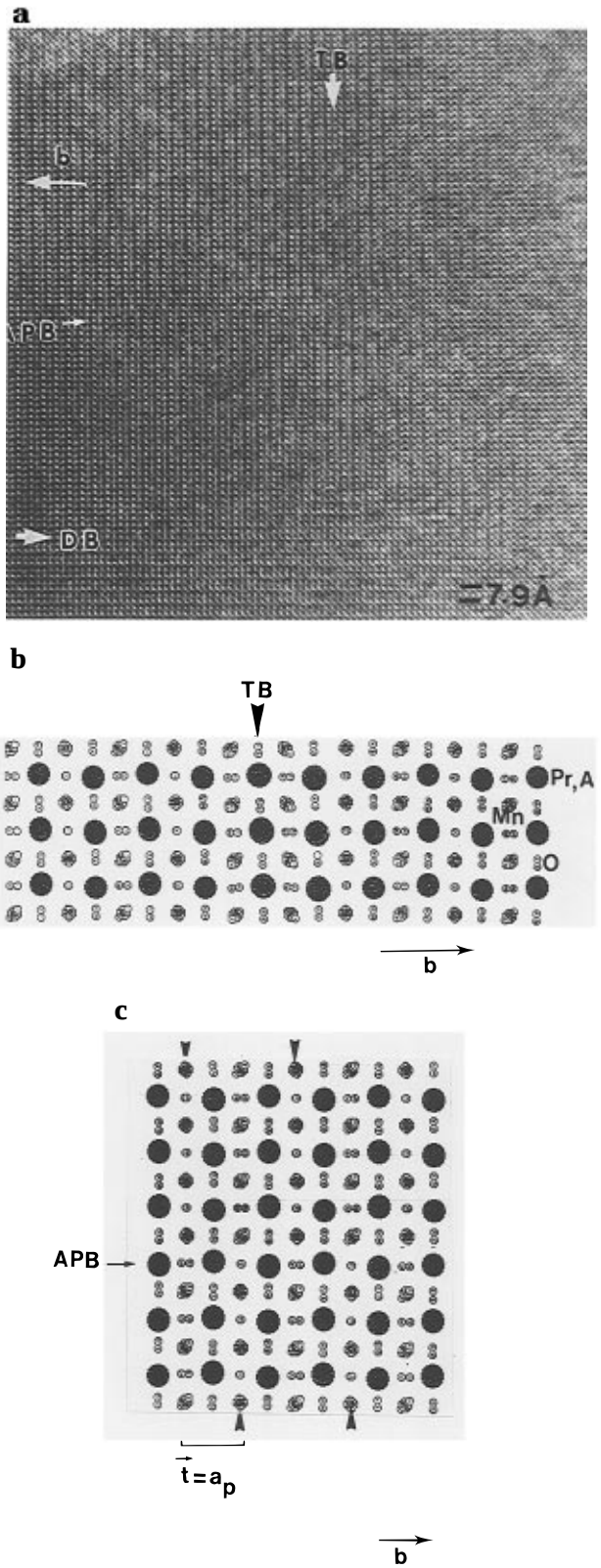

Figure 6. (a) Enlarged [101] image where three types of boundaries are observed: domain boundaries (BD), antiphase boundaries (APB), and twin boundaries (TB). Projections along [101] of the atom positions through (b) the twin boundary and (c) the antiphase boundary.

parameters determined for the deposition of the best films (film $F_{0.5}$). (ii) Film F_{1dec}: retaining $p_{O_2} = 1\%$, the temperature decrease mode was modified. (iii) Film F_{1ann}: applying postsynthesis annealings.

Since these three films are of worse quality than the optimized $F_{0.5}$, the nanostructural features are not detailed here. Only the main characteristics are presented.

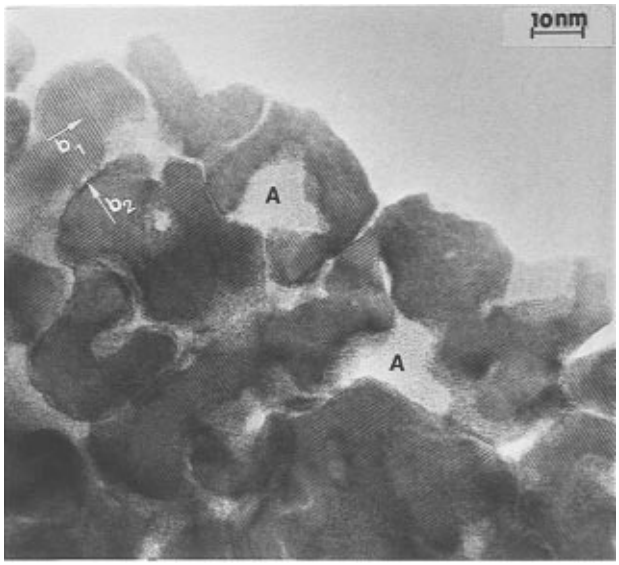

Figure 7. [101] image of the film F_1 (oxygen composition 1%): the structure of the crystallized grains is similar to that observed in the optimized film but amorphous areas (labeled A) are observed at the grain boundaries.

Increasing the oxygen pressure during the deposition, i.e., $p_{O_2} = 1\%$ instead of 0.5% (film F_1), does not modify the structural type of the manganite, but the grain boundaries are strongly damaged. A typical example is displayed in Figure 7. The contrast of the image is exactly similar to that observed for the optimized films and indicates that the structure remains unchanged. However, the difference between the two films deals with the fact that large areas of amorphous material are now located at the level of the grain boundaries (two areas are labeled A). The domain size and shape are roughly unchanged. The XRD pattern shows no change in peak positions but the intensity of the reflections (relative intensity film/substrate) decreases.

Suppressing the 30 min O_2 annealing (film F_{1dec}) and working again under a $p_{O_2} = 1\%$ partial oxygen pressure involve another strong modification of the film. This is first observed in the electron diffraction patterns. An example is given in Figure 8a. The intense reflections are those of the perovskite subcell, but a complex arrangement of extra reflections is observed. Such ED patterns can be interpreted from the superposition of five systems, all being directly related to the perovskite structure. The first two are [101] domains that are oriented 90°, i.e., the same domains as in the optimized films (labeled 1 and 2). The third type of domains are [010] domains (labeled 3), which seem to be more important in size since the rather intense reflections appear at positions $^1/_2,0,^1/_2$ with regard to the cubic subcell. The two last systems correspond to 90° oriented variants (indicated by a white triangle and labeled 4) of an original superstructure. This new supercell is orthorhombic and exhibits a doubling of the *c* axis, i.e., $a_4 \approx \sqrt{2}a_p$ and $c_4 \approx 2\sqrt{2}a_p$. The periodicity along b_4 is a_p or $2a_p$; it cannot be determined by electron diffraction due to the superposition of the different systems. The $c_4/2\sqrt{2}$ ($\approx a_p$) value of the supercell is slightly shorter than the $c/\sqrt{2}$ ($\approx a_p$) value of the parent structure, showing that the superstructure is correlated to a contraction along that direction. Note that the extra

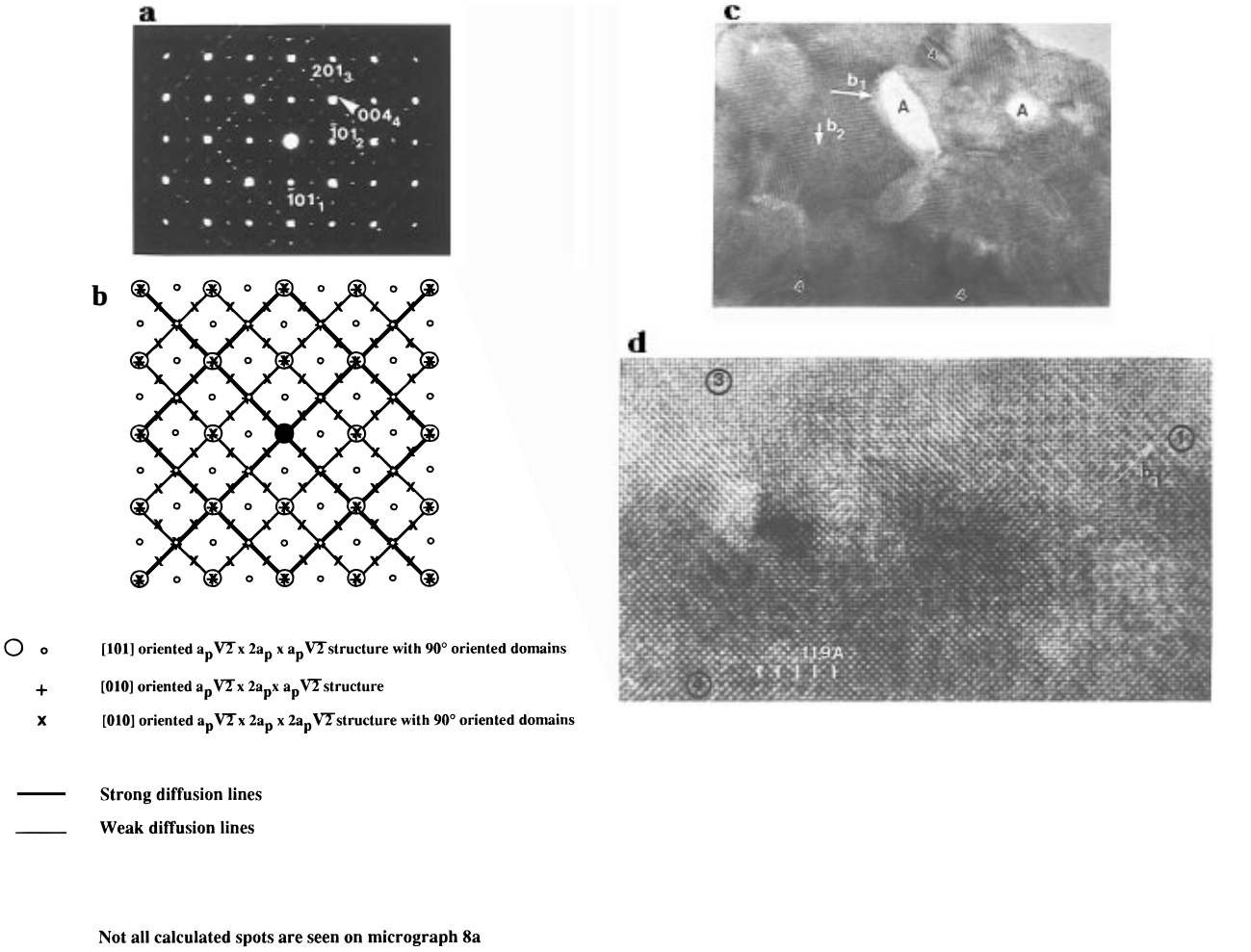

Figure 8. Film F_{1dec}: (a) [101] ED pattern which results from the superposition of five systems. Two 90° oriented domains of the [101] manganite (labeled 1 and 2). [010] are labeled 3). The orthorhombic supercell with $\sqrt{2}a_p \times 2a_p \times 2\sqrt{2}a_p$ is labeled 4 and exhibit also 90° oriented domains. (b) Schematic diffraction pattern indicating the different structures or orientations which correspond to the Figure 8a diffraction pattern. (c) Corresponding [101] overall images. A indicates amorphous areas, and 4 zones where the superstructure is established. (d) Enlarged image showing the coexistence of three types of domains.

reflections along c_4* are sometimes diffuse, suggesting that the ordering phenomenon that generates this superstructure is not perfectly periodic.

The corresponding overall image is given in Figure 8c. One observes the classical 90° oriented grains and the amorphous areas (labeled A) which have been observed in Figure 7. Comparing the optimized films ($F_{0.5}$) with F_1 and F_{1dec} shows clearly that the damaging of the grain boundaries through the formation of amorphous or ill-crystallized areas can be considered as characteristic of a too-high oxygen pressure during the film deposition.

The domains labeled 4 are those exhibiting a doubling of the c axis; the average periodicity along c_4 is mainly $2\sqrt{2}a_p \approx 11.9$ Å but local periodicities with $3\sqrt{2}a_p$ are also observed. The coexistence of these different values generates the streaks along c_4*. The enlarged HREM images recorded on the thin edges of the grains clearly show that the contrast remains typical of a perovskite throughout the whole matrix, whatever the periodicity of the superstructure is. This is shown in Figure 8d where three types of domains are observed. In the area labeled 4, the periodicity $2\sqrt{2}a_p$ is observed which clearly results only from a small local modulation of the contrast without a strong modification of the perovskite-type contrast. This suggests that the orthorhombic supercell, $\sqrt{2}a_p \times 2a_p \times 2\sqrt{2}a_p$, is not generated by a drastic atomic rearrangement but rather corresponds to a different distortion of the layers of MnO_6 octahedra. In the thicker part of the film, the corresponding domains (labeled 4 in Figure 8c) often exhibit an oval shape a few nanometers long. The boundaries between these domains and the matrix often appear as strained; this could be originated by the parameter mismatch (between c and c_4). The domain labeled 3 is characteristic of a [010] orientation of the manganite.[15] In the area labeled 1, the $2a_p$ periodicity is observed, corresponding to a [101] orientation and the contrast is that observed for the bulk material and in the optimized film $F_{0.5}$. These two types of domains have been described above.

Applying a postsynthesis annealing (850 °C under oxygen flow for 9 h) to F_1 leads to strong modifications of the films. The ED pattern recorded along the direction perpendicular to the substrate is given in Figure 9a. It can be easily interpreted by the superposition of four systems. Three systems are similar to those observed in $F_{0.5}$ (Figure 2a) and F_1 and consist of the superposition of three differently oriented grains of the classical manganite: [101] grains which exhibit perpendicular b_1 and b_2 axes in the plane parallel to the substrate and a few (considering the weakness of the $h0l$ reflections, indicated by a small arrow) grains are [010] oriented. The last and new system involves

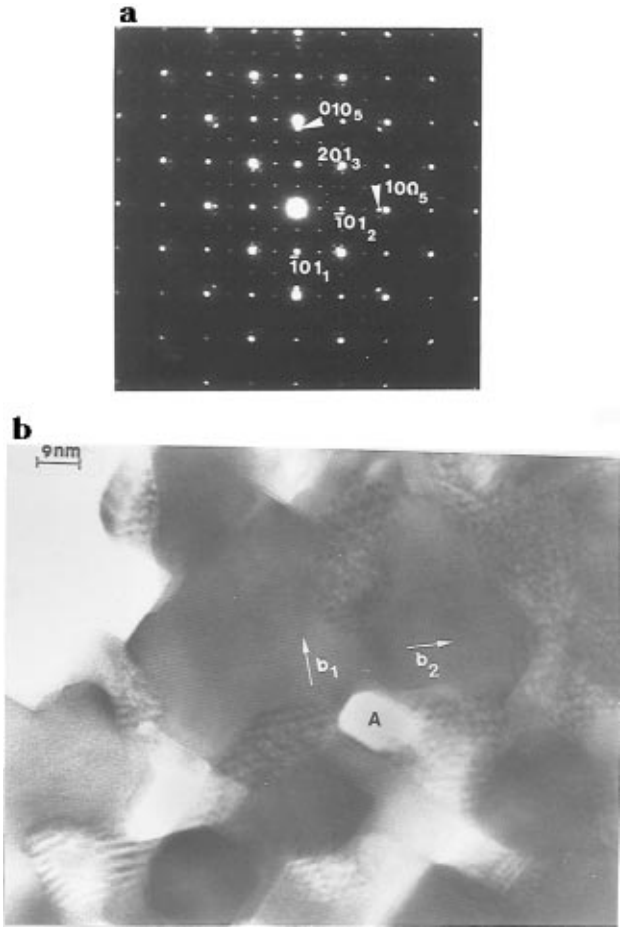

Figure 9. Film F_1: (a) [101] ED pattern. The [101] and [010] oriented domains of the manganites (labeled 1−3). The additional system (labeled 5) corresponds to a pseudo-cubic cell with a parameter close to 4.2 Å. (b) Corresponding [101] image. The Moiré patterns result from the superposition of the manganite structure with the cubic one, located at the grain boundaries.

the presence of extra reflection with $a_5 \approx b_5 \approx 4.2$ Å. The a_5 and b_5 axes are parallel to the a_p and b_p axes of the cubic perovskite subcell of the manganites, i.e., [010] and [101] direction of the orthorhombic cell. These extra reflections (indicated by white triangles) are rather strong, and weak extra satellites are observed as a result of double-diffraction phenomenon. The XRD pattern of this film is very similar to that registered for F_1; the only difference is the significant increase of the reflection intensity. From XRD patterns, the c_5 parameter seems to be very close to c_p.

The corresponding HREM images confirm the rectangular shape of the grains and the majority [101] oriented grains. An example is given in Figure 9b. The grain boundaries are of poor quality as for F_1, but it clearly appears that the new phase (characterized as the fourth system by ED) takes specifically place at the level of the grain boundaries. The correlated orientation (a_5 and b_5 parallel to [010] or [101]) and the parameter mismatch (3.85 and 4.2 Å) lead to the formation of Moiré patterns which are systematically observed at the grain boundaries (Figure 9b). The increase of the reflection intensities in the XRD pattern is easily explained considering that the amorphous areas are now crystallized.

Magnetic Behavior of the Films. Magnetic measurements were carried out in magnetic fields up to 5 T with B parallel to the substrate. Since the film signal

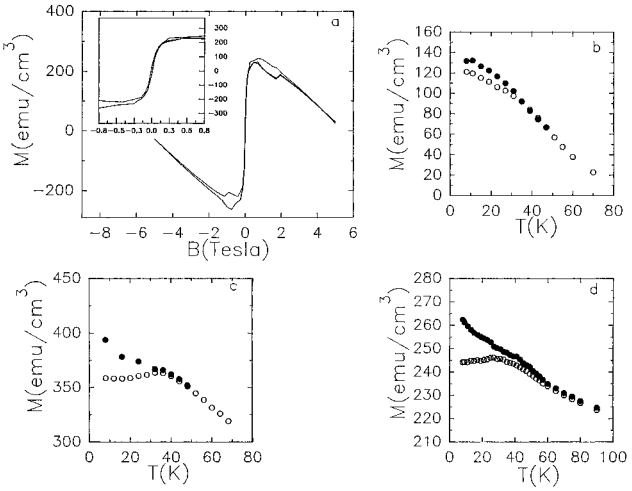

Figure 10. (a) Magnetization loop registered at 30 K for a $Pr_{0.7}Ca_{0.22}Sr_{0.08}MnO_{3-\delta}$ film. The insert shows the hysteresis at low field which is more pronounced for $B > 0.15$ T. (b−d) Temperature dependence of the magnetization for three different films: (b) $Pr_{0.7}Ca_{0.25}Sr_{0.05}MnO_{3-\delta}$. (c) $Pr_{0.7}Ca_{0.22}Sr_{0.08}MnO_{3-\delta}$ postannealed at 850 °C. (d) $Pr_{0.7}Ca_{0.22}Sr_{0.08}MnO_{3-\delta}$ as grown.

is rather small and the background signal due to the substrate and the sample holder rather large, hysteresis cycles were performed at low temperature in order to evidence a ferromagnetic behavior. A hysteretic behavior is observed which is more pronounced for $B > 1500$ G than around $B = 0$ G (Figure 10a), as is sometimes observed in bulk samples.[19] The value of the momentum measured in the films (about 400 emu/cm^3 for about 700 Å thickness) corresponds to 65% of the predicted 3.7 μ_b/Mn atom. The present lack of accuracy on the film thickness does not allow us to determine if it is due to experimental uncertainties or to a real spin canting of the phase (the decrease of $M(B)$ at high fields is due to the diamagnetism of the addenda which has to be subtracted from the signal). Moreover, the film is made of very small domains with the easy axis of magnetization which are not all aligned with the orientation of the field, so that no accurate determination of the momentum is possible. To monitor the variation of the hysteresis versus temperature, we measured the magnetization at 0.5 T in the first magnetization curve (zero field cooled, ZFC) and on the second branch of the cycle (Figure 10b−d). The Curie temperature T_c is between 35 K ($Sr_{0.05}$) and 60 K ($Sr_{0.08}$). This is much lower than similar results obtained in bulk samples (120−140 K).[20] The resistivity was measured with a four-probe method and the magnetoresistance behavior was measured at 65 K with an electrometer. Figure 11 presents a typical temperature dependence of the resistivity measured on our $Pr_{0.7}Ca_{0.3-x}Sr_xMnO_{3-\delta}$ films. All the films are semiconductor down to 5 K with an activation energy of 130 meV. This semiconducting behavior has been observed, with the same activation energy, on bulk $Pr_{0.7}Ca_{0.3-x}Sr_xMnO_{3-\delta}$ series for $x \leq 0.04$ compositions which have the lowest T_c (60 K), but for $x \geq 0.04$ an insulator metal transition is observed at temperatures close to T_c. In the inset (Figure 11), the magnetoresistive behavior is presented, showing a 35% decreases at

(19) Maignan, A.; Simon, C.; Caignaert, V.; Raveau, B. *J. Magn. Magn. Mater.* **1996**, *152*, L5.
(20) Maignan, A.; Simon, C.; Caignaert, V.; Raveau; B. *Z. Phys. B* **1996**, *99*, 305.

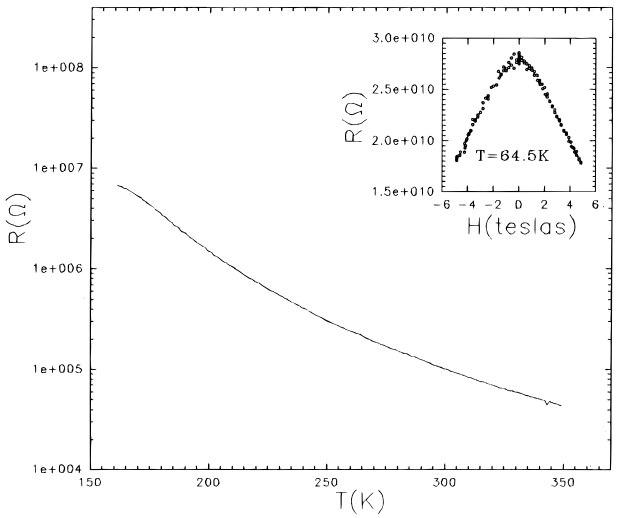

Figure 11. Temperature dependence of the resistivity for a $Pr_{0.7}Ca_{0.22}Sr_{0.08}MnO_{3-\delta}$ film. The insert shows the field dependence of the resistivity registered at 64.5 K with an electrometer. The magneto resistance ratio $(R_0 - R_{5T})/R_0$ is about 35%.

5 T. The annealing of the sample does not change this behavior qualitatively, but only quantitatively (15% before annealing, 35% after annealing). This result is very different from the GMR effect of the corresponding bulk sample (10^8 at the corresponding temperature). This disappointing result remains to be explained.

Different explanations can be proposed. The first is the presence of the numerous grain boundaries, which result from the very small size of the grains, contrary to the bulk sample where large crystals are observed. If the grain boundaries are not GMR, they are always semiconducting and would dominate the resistivity, even in the metallic phase of the center of the grains (the majority of the sample). Only control of the growing process could solve such a problem. Another interpretation can be invoked: If a difference of cationic composition can be ruled out, the cell parameter or the charge transfer (due to oxygen deficiency) could be different from the bulk sample. It was shown in bulk samples[10] that both parameters are very important on the GMR properties. It was also proposed that the size of the grains[21] is a key parameter for GMR properties.

Each of these explanations can be tested by different experiments such as changing the substrate (for the unit-cell parameter), oxygen annealing (for the charge transfer), or varying growth conditions (for the grain size). More work is needed to answer unambiguously this question.

Concluding Remarks

This study shows that $Pr_{0.7}Ca_{1-x}Sr_xMnO_3$, $x = 0.05$ and $x = 0.08$, manganites can be deposited in the form of thin films by rf magnetron reactive sputtering. The EDS analyses confirm that the film composition is that of the target so that all the species are properly transported. Provided the growth conditions have been optimized, their structure is exactly similar to that obtained for the bulk materials. The films consists of rectangular shaped grains which are preferentially [101] oriented, i.e., the $[\bar{1}01]$ direction is perpendicular to the substrate plane so that [101] and [010] are parallel to the *a* and *b* axes of the perovskite subcell. The HREM study shows that there are no extended defects in the bulk, only twin and antiphase boundaries which can be interpreted as resulting from the orthorhombic distortion.

The characteristics of the different films resulting from a modification of the growth parameters are of interest. A negative effect of the oxygen partial pressure has been evidenced, which involves a damaging of the grain boundaries: this effect is observed as soon as the O_2 pressure is too high, whatever the other growth parameters can be. If the in situ annealing under oxygen which is laid down at the end of the process is suppressed, the [010] orientation of the grains is favored and another superstructure is observed. From the HREM study, the new superstructure is directly related to the orthorhombic cell of the manganite. Different manganese-based oxides have been reported with ordered perovskite structures, exhibiting similar supercell parameters, $\sqrt{2}a_p \times 2a_p \times 2\sqrt{2}a_p$. In $CaMnO_{2.5}$, the superstructure described by Reller[22] results from an oxygen vacancies ordering. Such a supercell is also observed for the low-temperature form of the $Ln_{0.5}A_{0.5}MnO_3$.[12] Structural considerations, based on charge balance on one hand and on parameter values on the other hand, suggest that the mechanism engaged in the thin film is different. Postsynthesis annealings lead to the formation of a new phase that exhibits a periodicity close to 3.9 Å along the direction perpendicular to the substrate plane but with in-plane parameters significantly longer than those of the perovskite subcell. The significant parameter increase suggests a strong modification of the cationic composition as a result of the recrystallization of the amorphous phase located at the grain boundaries in the films prepared under high oxygen partial pressure.

As a conclusion, these structural and microstructural analyses evidence several important features for the manganite thin-film deposition that can be summarized as follows:

Cationic compositions can be perfectly controlled, so that the high sensitivity of the physical properties to parameters such as the average size of the cation in 12 fold coordination, can be expected to be tested in thin-film materials.

Film orientation is [101] in a reproducible way. This point could be important for further device applications.

Great similarities of the structural and nanostructural state of the film and bulk materials. These results allow us to discard different hypotheses for the magnetic behavior.

The high sensitivity of the film morphology to the oxygen pressure.

The understanding of the role of the oxygen content, by now decreasing oxygen pressure, and the domain size is in progress.

CM960572B

(21) Mahesh, R.; Mahendiran, R.; Raychaudhuri, A. K.; Rao, C. N. R. *Appl. Phys. Lett.* **1996**, *68*, 2291.

(22) Reller, A.; Thomas, J. M.; Jefferson, D. A.; Uppal, M. K. *Proc. R. Soc. London A* **1984**, *394*, 223.